Macroporous Bioglass Scaffolds Prepared by Coupling Sol–Gel with Freeze Drying

ARTICLE *in* CHEMISTRY OF MATERIALS · APRIL 2011

Impact Factor: 8.35 · DOI: 10.1021/cm103362c

2 AUTHORS, INCLUDING:

Matías Jobbagy
University of Buenos Aires
91 PUBLICATIONS **1,394** CITATIONS

CHEMISTRY OF MATERIALS

ARTICLE

pubs.acs.org/cm

Macroporous Bioglass Scaffolds Prepared by Coupling Sol−Gel with Freeze Drying

Yanina Minaberry[†] and Matías Jobbágy*[,†,‡]

[†]INQUIMAE-DQIAQF, Facultad de Ciencias Exactas y Naturales and [‡]Centro Interdisciplinario de Nanociencia y Nanotecnología, Universidad de Buenos Aires, Ciudad Universitaria, Pab. II, C1428EHA Buenos Aires, Argentina

Supporting Information

ABSTRACT: Free-standing macroporous bioglass scaffolds were prepared by a sol−gel route. The ice-segregation-induced self-assembly method was employed to structure a bioglass aqueous sol in the form of green monoliths with a well-defined macroporosity. The achieved texture was essentially preserved after a mild annealing at 873 K. The texture can be properly tuned by typical variables such as the freezing rate or sol concentration. In addition to these physical preparative variables, the acidity level plays a key role in preventing the silica condensation, keeping the primary building units in the early stages of the sol−gel transition and allowing the obtainment of large macropores. The chemical homogeneity of the resulting bioglass was enough to ensure a proper in vitro biomineralization response, resulting in a well-distributed hydroxyaopatite-like nanoparticulated layer.

KEYWORDS: biomineralization, porous materials, glasses, sol−gel

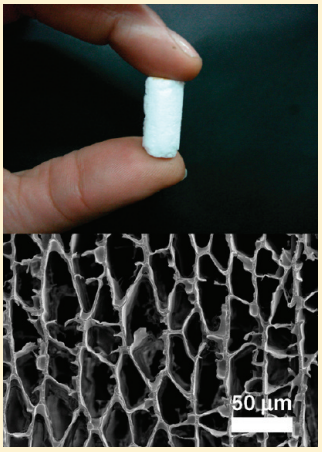

INTRODUCTION

Bone-repair engineering is a permanent source of inspiration for the materials science community. The first step to emulate bones was based on the preparation of synthetic calcium phosphate phases. Later on, nonnatural occurring synthetic phases based on silica, known as bioactive glasses or bioglasses, exhibited outstanding properties for bone reconstruction.[1,2] Several formulations based on silicon(IV), phosphorus(V), calcium(II), and alkaline oxides were proposed in order to maximize bioactivity, which is defined as the ability of the material to bond to bone tissue via the formation of a bone-like hydroxyapatite (HA) layer on its surface.[1] These new chemical platforms revealed an enhanced angiogenesis ability[3,4] and upregulation of specific genes that control the osteoblast cell cycle,[5,6] among other relevant characteristics.[7] Nowadays, efforts are pointed at building up either bioglasses or calcium phosphates in the form of sophisticated architectures,[8] in order to enhance their regeneration ability because the cell culture is induced to self-assemble into a three-dimensional (3D) tissuelike structure with the aid of 3D biodegradable and biocompatible scaffolds. Textural properties, in particular macroporosity, must be tuned to achieve a well-interconnected pore network, in order to allow not only cell proliferation within the materials but also proper mass transport between it and the surrounding physiological media.[9−12] In this sense, many approaches to texture bioglasses were proposed, depending on the desired form and/or porosity, including in situ foam generation,[13] sacrifice template filling,[14] electrospinning,[15] or robotic deposition,[16] and gave birth to a variety of 3D architectures.

In recent years, the ice-segregation-induced self-assembly (ISISA) method has arisen as a unique tool for the construction of porous monoliths, allowing sophisticated control of the macroporous texture, in terms of the pore size, shape, distribution, and orientation. The process involves the submission of an aqueous gel, solution, or suspension to liquid-nitrogen temperatures. The controlled ice formation, typically in the hexagonal form, drives the segregation of every solute or colloid originally dispersed in the aqueous phase toward the zones in which the ice is absent, giving rise to a hierarchical assembly either defined by walls, fibers, or bicontinuous arrays of matter surrounding empty areas where the ice resided before sublimation, resulting in an organized 3D scaffold. This process holds a promissory future because it can texture large pieces, in the range of centimeters, with pores aligned in a preferential direction.[17−19] From a chemical point of view, diverse monoliths or scaffolds ranging from strictly ceramic phases[19−23] to living-cell loaded polymers[24] or even carbon nanotube networks[25] can be obtained by this process.[26]

Sol−gel-based procedures, in contrast with traditional ceramic methods, allow for the preparation of outstanding bioglasses because silica polymerizes in an intimate mixture with phosphate and calcium ions, preventing the massive segregation of calcium phosphate. In contrast with ceramic methods, the low annealing

Received: November 23, 2010
Revised: March 29, 2011
Published: April 14, 2011

temperatures employed also allow for the preparation of even mesoporous pores without sintering, giving rise to new bifunctional bioglasses with advanced drug-carrier or enhanced blood-coagulation properties.[27−30]

The aim of the present work is to demonstrate that sol−gel procedures, coupled with the ISISA texturing method, allow for the preparation of free-standing bioglass monoliths, with tunable porosity. The effect of the main preparative variables on the final texture, as well as the in vitro biomineralization ability, is explored.[21,22]

EXPERIMENTAL SECTION

Materials. Analytical-grade $Ca(NO_3)_2 \cdot 4H_2O$, triethyl phosphate (TEP), 65% HNO_3, and tetraethoxysilane (TEOS) were received from Aldrich, Germany, and used without further purification.

Preparation of Aqueous Silica−TEP Stock Solutions. The silica−TEP sol was obtained by hydrolyzing 10.26 g of TEOS and 0.56 g of TEP in 3.84 mL of HNO_3 (0.06 M). The sol was vigorously stirred at room temperature for 1 day and then mixed with an equal volume of water. Ethanol was removed under reduced pressure (40 °C, 30 mbar) until the weight loss corresponded to the amount of ethanol resulting as a byproduct of the TEOS and TEP hydrolysis reaction.

Immediately after ethanol removal, bioglass−sol precursors were obtained by mixing 0.47 mL of the aqueous silica−TEP sol, 0.11 mL of $Ca(NO_3)_2 \cdot 4H_2O$ (saturated solution), and 0.78 mL of water, reaching a final 15:5:80 molar ratio of $Ca^{II}/P^{V}/Si^{IV}$. An extra amount of water was added to obtain a final lower bioglass concentration than was required.[10] After an aging step of 24 h at room temperature, the gelled precursors were submitted to ISISA. Processing of ISISA: Once loaded into the molds, typically insulin syringes (length 80 mm; diameter 4 mm), the fresh bioglass−precursor sols were unidirectionally frozen by dipping the molds at defined rates into a cold −196 °C (liquid-nitrogen) bath. The unidirectionally frozen samples were freeze-dried using an Alpha 1-2 LD Plus freeze-drier. The green monoliths were finally annealed at 873 K (10 K min^{-1}) and held at the final temperature for 5 h.[31]

The pore dimensions and wall thickness of the monoliths were determined from scanning electron microscopy (SEM) micrographs of cross sections to the direction of freezing. For each construct, at least 20 measurements of the pore width and wall thickness were made on each micrograph, to provide a representative mean value and standard deviation.

Mechanical Properties. Parallel-plate compression tests were carried out on cylindrical scaffolds, with heights of 20 mm and diameters of 10 mm using an Instron testing machine (model 5569A) with a crosshead speed of 10 mm min^{-1} and a 1000 N load cell. Five specimens for each sample group were tested to obtain the average value along with its standard deviation.

In Vitro Bioactivity Test. The assessment of the in vitro bioactivity of the annealed scaffolds was carried out in a simulated body fluid (SBF) solution composed of NaCl (137.5 mM), KCl (3.02 mM), $K_2HPO_4 \cdot 3H_2O$ (1.01 mM), $MgCl_2 \cdot 6H_2O$ (1.53 mM), $CaCl_2$ (2.63 mM), and Na_2SO_4 (0.51 mM) in distilled water and buffered at pH 7.3 with tris(hydroxymethyl)aminomethane [$(HOCH_2)_3CNH_2$, 50.5 mM] and HCl.[32] Each specimen (0.1 g) was immersed in 100 mL of SBF contained in polyethylene vials and incubated at 37 °C under sterile conditions for 1−4 weeks. Once removed from the incubation solution, the samples were rinsed gently first in ethanol and then in deionized water and left to dry at ambient temperature in a desiccator for further characterization. The sample's evolution was analyzed by SEM (Zeiss Supra-40), coupled with energy-dispersive spectroscopy (EDS) and Fourier transform infrared (FTIR; Nicolet 8700 20 SXC). Powder X-ray diffraction patterns (PXRD) were recorded in the 2θ range of 10−40°, with a step size of 0.02° and a step time of 2 s, under reflection mode with a Siemens D5000 device, employing Ni-filtered Cu Kα radiation. Evolution of the SBF composition was followed in terms of the pH and calcium(II) and phosphorus(V) concentrations by means of a pH meter (Schott) and inductively coupled plasma atomic emission spectroscopy, respectively. Thermal analysis was performed using in a Shimadzu TG50 in air with a heating rate of 10 °C min^{-1} under an air flow (50 mL min^{-1}).

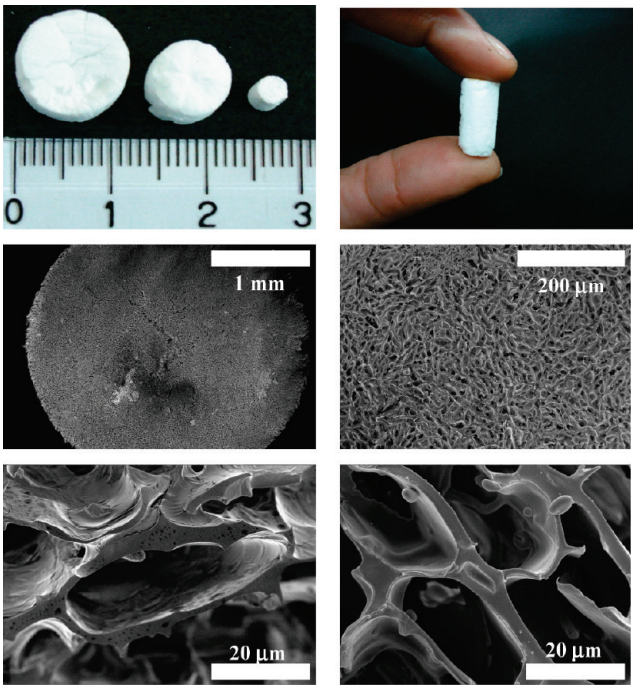

Figure 1. SEM images of a cross-sectioned (perpendicular to the direction of freezing) monolithic scaffold prepared with a solid content of 7 wt % and a freezing rate of 1.5×10^{-2} mm s^{-1}. Lower images depict detail of the wall's texture before the green scaffold (left) and the sample annealed for 5 h at 873 K (right).

RESULTS AND DISCUSSION

It is known that the versatility offered by the ISISA process lies in the possibility of tuning the monolith's texture with several physicochemical parameters, such as the solvent composition, the solute nature and concentration, the freezing rate, and the temperature gradient.[26] In the present study, the preparation of bioglass monolithic scaffolds was restricted to the use of water as the solvent and the thermal gradient will be established between ambient (298 K) and liquid nitrogen (77 K). Concerning the sample composition, a well-accepted Ca/P/Si bioglass formula[33] was chosen, focusing this study on the textural modification, exclusively. Then, a family of bioglass precursors (green scaffolds in the following) was prepared by means of increasing the solid contents and/or freezing rates. Figure 1 (upper row) presents a series of monoliths prepared under typical conditions inside cylindrical molds. The resulting monoliths kept both the shape and size of the parent container in which the parent sols were confined prior to ISISA. Because the ice-front progress state reached a stationary value (e.g., nominal) at the upper half of the monolith, the characterization and experiments were always conducted on that portion.[34] SEM inspection of their transversal section revealed a homogeneous texture, with the pore pattern being only slightly altered in a small region a few micrometers

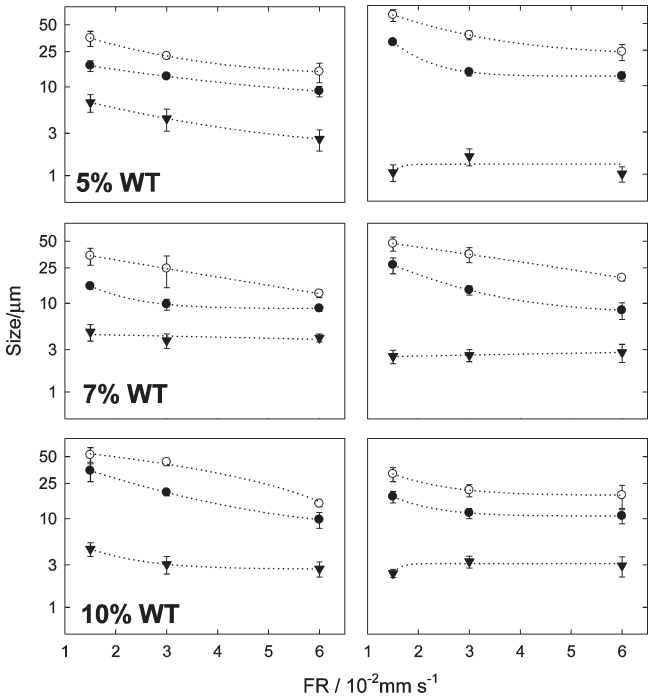

Figure 2. Evolution of the pore's dimensions: major (○) and minor (●) lengths and wall thickness (▼) of scaffolds prepared with increasing solid content and freezing rates, before (left column) and after (right column) annealing for 5 h at 873 K.

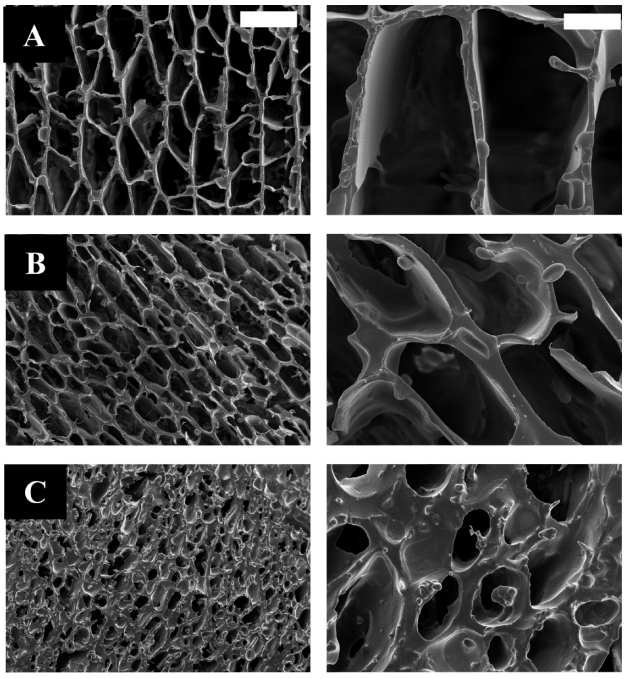

Figure 3. SEM images of cross-sectioned (perpendicular to the direction of freezing) monolithic scaffolds annealed for 5 h at 873 K, prepared at solid contents and freezing rates of 5 wt %, 1.5×10^{-2} mm s^{-1} (A), 7 wt %, 3×10^{-2} mm s^{-1} (B), and 10 wt %, 6×10^{-2} mm s^{-1} (C), respectively. Left column: the scale bar equals 50 μm. Right column: the scale bar equals 10 μm.

from the external surface parallel to the freezing direction.[35] Figure 1 (middle row) shows a 3-mm-thick monolith mounted as a whole; the pores are randomly oriented, exhibiting dimensions of around 10 μm.

In contrast with related pure silica systems,[36] the lack of well-defined hexagonal pores, even for low freezing rates, could be ascribed to the effect of salts dissolved in the aqueous phase, which hinders the growth of well-defined pure water crystals. However, the obtained texture is well preserved all along the sample volume, without the occurrence of radial heterogeneity or massive cracks.[35]

It is worth mentioning that the green monoliths exhibited a secondary submicrometric porosity within the walls; these cavities are commonly seen in related systems (see Figures 1, lower row, and S1 in the Supporting Information).[35] A detailed inspection of the wall's texture revealed smooth surfaces with no evidence of segregation of micrometric calcium(II) phosphate phases. Typically, sol−gel-based bioglasses involve an oxidative annealing step in which the remnant salts, acid, and eventual organic moieties are decomposed. Additionally, this step involves the solid-state consolidation of the bioglass itself; on the basis of previous reports and in order to prevent a massive sintering and pore collapse, the annealing temperature was fixed at 873 K.[31,37] After a 5 h annealing process, these small pores collapse, with a marked densification of the walls and eventual wall contraction. The exposed surface of the inner part of the walls after the sample's fracture resembled glasslike ones of bare sintered silica. However, for highly concentrated sols, some of the intrawall voids were large enough, in the range of micrometers, to remain after the annealing step. Then, a SEM screening taking representative images of the obtained textures was performed before and after annealing at 873 K, in order to assess to which extent the original structure of the green scaffold is altered by sintering, depending on the preparation conditions.

Evolution of the most significant textural parameters of each sample was described by means of the pore's major and minor dimensions and the wall thickness. Figure 2 compiles the evolution of the aforementioned parameters observed for the green scaffolds and the corresponding annealed ones, prepared under different conditions. Figure 3 shows SEM images of representative textures observed for this family of samples, after annealing at 873 K.

In general terms, the green scaffold's texture follows the expected trend, in which the freezing rate exerted a marked influence on both the pore size and shape. The wall thickness remains 1 order of magnitude smaller than the pore size, achieving a cellularlike aspect. Low rates allow the formation of bigger ice crystals, giving birth to oblong pores with longer dimensions and almost doubling the shorter one; then both dimensions were taken into account. The more ordered texture resembles the typical parallel lamellae periodically segmented by perpendicular secondary bridges, commonly observed in related systems.[38] The magnitude of supercooling depends on the ice-front rate; faster freezing rates favor a supercooling zone in an unstable situation, hindering the formation of large ice crystals and resulting in a scaled down microstructure. For a faster employed freezing rate, the pores dramatically collapse into less defined forms, tending to a bicontinuous phase in which pores and walls exhibit similar dimensions and morphology.

Once the monoliths are annealed, their macroscopic dimensions are almost preserved; however, the micrometric texture, depending on the preparation conditions, can be significantly altered. In Figure 2 (left column, 5 wt %), a marked wall

dx.doi.org/10.1021/cm103362c |Chem. Mater. 2011, 23, 2327–2332

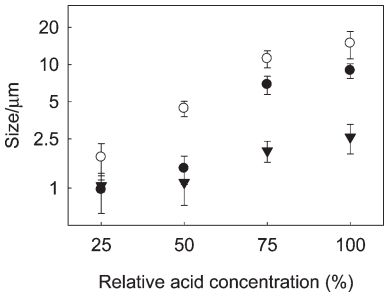

Figure 4. Evolution of the pore dimensions (larger ○, shorter ●) and the average wall thickness (▼), as a function of the initial acid concentration for solutions containing 10 wt %, prepared with a freezing rate of 6×10^{-2} mm s^{-1}, annealed at 873 K.

contraction of several micrometers can be observed. Because this contraction is not extended to the macroscopic piece, the pores expand after annealing. This effect is less marked for intermediate rates and/or compositions, and for the highest rates and concentrations, the annealed and nonannealed walls are almost indistinguishable.

With the influence of the typical preparative parameters being established, we focused our attention on key chemical aspects related to the proposed method. Beyond the freezing rate or solid content, the ISISA process is significantly affected by the inherent nature of the involved solutes. In general, for certain freezing conditions, both the solute diffusion coefficient and inherent solubility affect the spatial frequency in which the ice crystals, say the pores, occur.[21] This fact is particularly relevant for structuring purposes; for example, solutions containing poly(vinyl alcohol) with increasing molecular weights can develop interpore average distances varying from 1 to 20 μm.[35] In the case of sol−gel-based ISISA, instead of initially defined polymeric macromolecules, the starting silica sol provides the primary building units of the green scaffold. The degree of condensation of that silica sol, which depends on the time, pH, and temperature, among other factors, rules the average size of the primary nanoparticles. It was demonstrated that the mobility of silica (silica framework in hydrogels or silica particles in hydrosols) governs the resulting shape; because the mobility of silica is restricted, it assembles in the form of lamella, flat fiber, microhoneycomb, fibers with polygonal cross sections, or even powders.[20]

In the present case, for a given silica concentration in the starting sol, the silicon(IV) to proton ratio is the chemical parameter that will govern the silica condensation rate.[39] Given a certain time after the bioglass sol is prepared, the more acidic the starting sol, the smaller and more mobile the silica polymers, say the primary building units. Then, in order to assess to which extent this preparative variable could affect the present procedure, samples prepared with sols aged for 1 h and with decreasing acid content were submitted to ISISA under identical freezing conditions. The acid content range was kept high enough to prevent massive segregation of the calcium(II) phosphate phases before ISISA.[20] Even for the lowest acid content, the absence of any diffraction pattern corresponding to calcium(II) and phosphorus(V) phases, as well as the occurrence of a broad reflection centered at $2\theta = 24°$, typical of amorphous silica, suggests the effective formation of a pure bioglass for all of the samples prepared. EDS-based elemental mapping confirmed the homogeneous distribution of both calcium(II) and phosphorus(V).

Figure 4 depicts evolution of the main structural parameters for a family of samples prepared with decreasing amounts of acid, taking the initially tested sol as a 100% acidity reference.

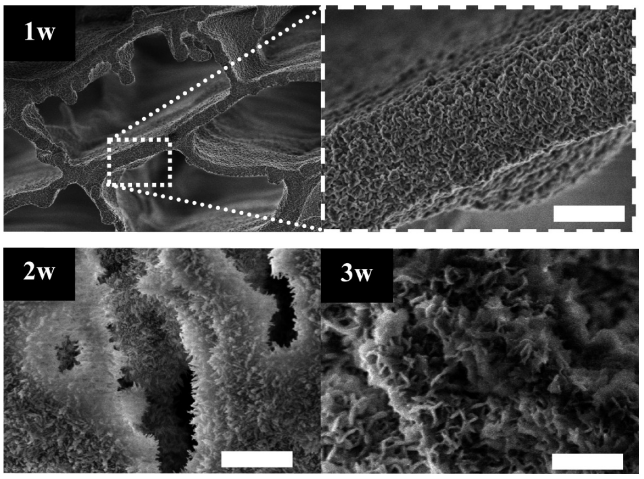

Figure 5. SEM images of cross-sectioned (perpendicular to the direction of freezing) monolithic scaffolds prepared with a solid content of 7 wt % and a freezing rate of 1.5×10^{-2} mm s^{-1}, exposed to SBF for 1−3 weeks (1w, 2w, 3w, etc.). Upper left: the scale bar represents 10 μm. All other bars represent 1 μm.

In the present case, the acidity plays a key role in the final texture, allowing tuning of the final pore size in almost a 10-fold factor. Even for the lowest acidity formulation, the textural influence of both the solid content and freezing rate follows the expected tendency (see Figures S4 and S5 in the Supporting Information).

The mechanical properties of representative samples were assessed by means of compression tests, exhibiting compressive strength ranging from 0.05 to 0.2 MPa, in good agreement with related highly porous sol−gel-based bioglasses (see Figures S6 and S7 in the Supporting Information).[11] The increment of the average wall thickness exerted by the acid content is also reflected in a slightly higher compressive strength. These values can be improved by increasing the calcination temperature to 800 °C (see Figure S8 in the Supporting Information); however, further annealing could result in lower bioactivity.[9]

MINERALIZATION BEHAVIOR

In order to evaluate the potential bioactivity of the obtained bioglass scaffolds, several representative annealed samples were submitted to a well-established in vitro bioactivity assay, based on the incubation of bioglasses in SBF at 37 °C (Figure 5). The samples were separated from the SBF solution, which was preserved for chemical analysis.

After 1 week of incubation, the original glasslike surface of the scaffolds turned rough because of deposition of a homogeneous layer of particles of ca. 50 nm. After the second week, those particles grew in the form of elongated needles, yet preserving a dense coverage onto the scaffold surface. Finally, after 3 weeks, larger flakelike particles replaced the former needles. The chemical nature of the deposited layer was estimated by means of a SEM−EDS probe applied over different regions of the scaffold; in all cases, the Ca/P ratio was ca. 1.6 ± 0.3, practically that of HA. PXRD inspection of the mineralized samples revealed the birth of a signal after 2 weeks in the form of a main peak centered at $2\theta = 32°$ and a less intense and sharper one positioned at $2\theta = 26°$, mounted over the broad background signal belonging to the bioglass substrate (see Figure 6). The former main peak can be

dx.doi.org/10.1021/cm103362c |*Chem. Mater.* 2011, 23, 2327–2332

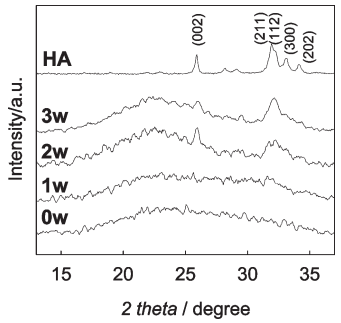

Figure 6. Evolution of PXRD patterns of a sample exposed to SBF for 1−3 weeks. The pattern recorded for commercial HA is also included.

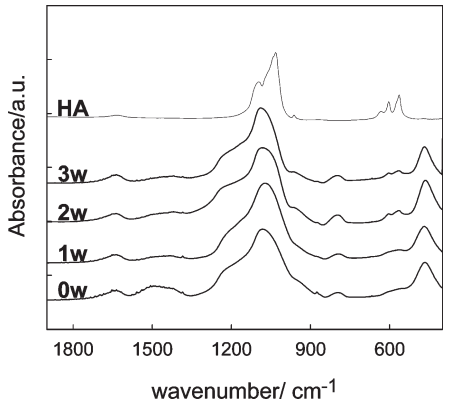

Figure 7. Evolution of FTIR spectra of a sample exposed to SBF for 1−3 weeks. The spectrum recorded from commercial HA is also included.

ascribed to the sum of the overlapped 211, 112, 300, and 202 reflections of HA, while the latter peak corresponds to the 002 one, exclusively (see the HA reference also included). As a control experiment, pure silica synthesized, as described above, without the addition of calcium(II) or phosphorus(V) in the formulation was also exposed to SBF. Even after 3 weeks, no signal of the HA-like layer was observed.

Evolution of samples exposed to SBF was inspected by means of FTIR spectroscopy analysis (Figure 7). The FTIR spectra showed main bands composed of signals centered at 950, 1100, and 1200 cm^{-1}, related to the Si−O−Si and P−O stretching of silica glass, and a shoulder at about 900 cm^{-1}, related to the Si−O−Ca vibrational mode. The peak centered at 450 cm^{-1} accounted for the Si−O−Si bending of silica glass.[40] After 2 weeks, a couple of well-defined additional peaks centered at 598 and 566 cm^{-1} became noticeable, corresponding to P−O bending vibrations of apatite-like phases (see the HA reference),[41,42] in good agreement with PXRD data. Then, the mineral layer could be ascribed to the desired HA-like one.

Typically, once bioglasses are exposed to SBF, a surface dissolution process is triggered. Then, both the calcium(II) and phosphorus(V) concentrations in solution continuously increase, increasing supersaturation with respect to HA up to a critical value, in which the nucleation and growth of that phase takes place on the exposed surface.[43] After that initial step, which usually takes 1 week for dense bioglasses,[9,44,45] the solution composition remains almost invariant, even when the HA layer is still developing.[43] However, being a mass-transport-affected process, the bioglass texture could influence biomineralization kinetics, as was reported for high-surface mesoporous bioglasses[46,47] or nanofiber-shaped ones,[15] in which the initial step can be reduced to several hours. Then, calcium(II)- and phosphorus(V)-released kinetics are a robust indication of surface reactivity. In the present case, the concentration profiles observed for samples with different solid or acid content were almost identical, indicating that neither variable affected the chemical response of the sintered bioglasses. For samples prepared with the same starting sol and exhibiting different porosities due to the freezing rate, their chemical behaviors were similar, suggesting that the transport properties are not controlling the biomineralization process under the explored conditions.

CONCLUSIONS

The ISISA-based texturization of sol−gel bioglass precursors opened the gate for the preparation of macropurous green monoliths with a well-defined macroporosity that was essentially preserved after mild annealing. The chemical homogeneity was enough to ensure a well-defined in vitro biomineralization response. In addition to the physical preparative variables, the sol−gel chemical process can also be tuned in order to modify the final structure, allowing the obtainment of large macropores. Because the freezing rate can be easily tuned and modified within a given sample, this process is promissory in the preparation of monolithic pieces with a porosity gradient,[48] which, in principle, should tune and control the cellular response to these scaffolds.[49,50]

ASSOCIATED CONTENT

Supporting Information. Details of the secondary porosity and other textural features. This material is available free of charge via the Internet at http://pubs.acs.org.

AUTHOR INFORMATION

Corresponding Author
*E-mail: jobbag@qi.fcen.uba.ar.

ACKNOWLEDGMENT

This work was supported by the University of Buenos Aires (UBACyT X-003), by the Agencia Nacional de Promoción Científica y Tecnológica (ANPCyT PICT 06-33973), and by the National Research Council of Argentina (CONICET PIP 112200801025332). We are deeply indebted to Dr. Andy Zelcer for his fruitful comments and to P. E. Rocci, C. E. Buyatti, and N. Rosic (INTI) and Dr. Celina R. Bernal (INTECIN) for their kind assistance during the mechanical tests. Y.M. acknowledges CONICET for a postdoctoral fellowship. M.J. is a Research Scientist of CONICET (Argentina).

REFERENCES

(1) Hench, L. L. *J. Mater. Sci.: Mater. Med.* **2006**, *17* (11), 967–978.
(2) Arcos, D.; Vallet-Regí, M. *Acta Biomater.* **2010**, *6* (8), 2874–2888.
(3) Day, R. M.; Boccaccini, A. R.; Shurey, S.; Roether, J. A.; Forbes, A.; Hench, L. L.; Gabe, S. M. *Biomaterials* **2004**, *25* (27), 5857–5866.
(4) Day, R. M. *Tissue Eng.* **2005**, *11* (5−6), 768–777.
(5) Xynos, I. D.; Edgar, A. J.; Buttery, L. D. K.; Hench, L. L.; Polak, J. M. *J. Biomed. Mater. Res.* **2001**, *55* (2), 151–157.

(6) Xynos, I. D.; Hukkanen, M. V. J.; Batten, J. J.; Buttery, L. D.; Hench, L. L.; Polak, J. M. *Calcif. Tissue Int.* **2000**, *67* (4), 321–329.
(7) Roether, J. A.; Boccaccini, A. R.; Hench, L. L.; Maquet, V.; Gautier, S.; Jerome, R. *Biomaterials* **2002**, *23* (18), 3871–3878.
(8) Gutiérrez, M. C.; Jobbágy, M.; Ferrer, M. L.; Del Monte, F. *Chem. Mater.* **2008**, *20* (1), 11–13.
(9) Jones, J. R.; Ehrenfried, L. M.; Hench, L. L. *Biomaterials* **2006**, *27* (7), 964–973.
(10) Ohtsuki, C.; Kokubo, T.; Yamamuro, T. *J. Non-Cryst. Solids* **1992**, *143* (1), 84–92.
(11) Rezwan, K.; Chen, Q. Z.; Blaker, J. J.; Boccaccini, A. R. *Biomaterials* **2006**, *27* (18), 3413–3431.
(12) Kokubo, T.; Kim, H. M.; Kawashita, M. *Biomaterials* **2003**, *24* (13), 2161–2175.
(13) Hall, S. R.; Walsh, D.; Green, D.; Oreffo, R.; Mann, S. *J. Mater. Chem.* **2003**, *13* (2), 186–190.
(14) Qian, J. M.; Kang, Y. H.; Wei, Z. L.; Zhang, W. *Mater. Sci. Eng. C: Biomim. Supramol. Syst.* **2009**, *29* (4), 1361–1364.
(15) Kim, H. W.; Kim, H. E.; Knowles, J. C. *Adv. Funct. Mater.* **2006**, *16* (12), 1529–1535.
(16) Yun, H. S.; Kim, S. E.; Hyun, Y. T.; Heo, S. J.; Shin, J. W. *Chem. Mater.* **2007**, *19* (26), 6363–6366.
(17) Deville, S.; Maire, E.; Lasalle, A.; Bogner, A.; Gauthier, C.; Leloup, J.; Guizard, C. *J. Am. Ceram. Soc.* **2009**, *92* (11), 2489–2496.
(18) Deville, S.; Maire, E.; Lasalle, A.; Bogner, A.; Gauthier, C.; Leloup, J.; Guizard, C. *J. Am. Ceram. Soc.* **2009**, *92* (11), 2497–2503.
(19) Deville, S.; Maire, E.; Bernard-Granger, G.; Lasalle, A.; Bogner, A.; Gauthier, C.; Leloup, J.; Guizard, C. *Nat. Mater.* **2009**, *8* (12), 966–972.
(20) Mukai, S. R.; Nishihara, H.; Tamon, H. *Microporous Mesoporous Mater.* **2008**, *116* (1−3), 166–170.
(21) Nishihara, H.; Iwamura, S.; Kyotani, T. *J. Mater. Chem.* **2008**, *18* (31), 3662–3670.
(22) Deville, S. *Adv. Eng. Mater.* **2008**, *10* (3), 155–169.
(23) Deville, S.; Maire, E.; Lasalle, A.; Bogner, A.; Gauthier, C.; Leloup, J.; Guizard, C. *J. Am. Ceram. Soc.* **2009**, *92* (11), 2489–2496.
(24) Gutierrez, M. C.; Garcia-Carvajal, Z. Y.; Jobbagy, M.; Yuste, L.; Rojo, F.; Abrusci, C.; Catalina, F.; del Monte, F.; Ferrer, M. L. *Chem. Mater.* **2007**, *19* (8), 1968–1973.
(25) Gutierrez, M. C.; Garcia-Carvajal, Z. Y.; Hortiguela, M. J.; Yuste, L.; Rojo, F.; Ferrer, M. L.; del Monte, F. *J. Mater. Chem.* **2007**, *17* (29), 2992–2995.
(26) Gutierrez, M. C.; Ferrer, M. L.; del Monte, F. *Chem. Mater.* **2008**, *20* (3), 634–648.
(27) Yan, X. X.; Yu, C. Z.; Zhou, X. F.; Tang, J. W.; Zhao, D. Y. *Angew. Chem., Int. Ed.* **2004**, *43* (44), 5980–5984.
(28) Lopez-Noriega, A.; Arcos, D.; Izquierdo-Barba, I.; Sakamoto, Y.; Terasaki, O.; Vallet-Regi, M. *Chem. Mater.* **2006**, *18* (13), 3137–3144.
(29) Arcos, D.; Lopez-Noriega, A.; Ruiz-Hernandez, E.; Terasaki, O.; Vallet-Regi, M. *Chem. Mater.* **2009**, *21* (6), 1000–1009.
(30) Ostomel, T. A.; Shi, Q. H.; Tsung, C. K.; Liang, H. J.; Stucky, G. D. *Small* **2006**, *2* (11), 1261–1265.
(31) Boccaccini, A. R.; Chen, Q.; Lefebvre, L.; Gremillard, L.; Chevalier, J. *Faraday Discuss.* **2007**, *136*, 27–44.
(32) Kokubo, T.; Takadama, H. *Biomaterials* **2006**, *27* (15), 2907–2915.
(33) Ohtsuki, C.; Kokubo, T.; Takatsuka, K.; Yamamuro, T. *J. Ceram. Soc. Jpn., Int. Ed.* **1991**, *99* (1), 2–7.
(34) Deville, S.; Saiz, E.; Tomsia, A. P. *Acta Mater.* **2007**, *55* (6), 1965–1974.
(35) Gutierrez, M. C.; Garcia-Carvajal, Z. Y.; Jobbagy, M.; Rubio, T.; Yuste, L.; Rojo, F.; Ferrer, M. L.; del Monte, F. *Adv. Funct. Mater.* **2007**, *17* (17), 3505–3513.
(36) Nishihara, H.; Mukai, S. R.; Yamashita, D.; Tamon, H. *Chem. Mater.* **2005**, *17* (3), 683–689.
(37) Arcos, D.; Greenspan, D. C.; Vallet-Regã, M. *Chem. Mater.* **2002**, *14* (4), 1515–1522.
(38) Hortiguela, M. J.; Gutierrez, M. C.; Aranaz, I.; Jobbagy, M.; Abarrategi, A.; Moreno-Vicente, C.; Civantos, A.; Ramos, V.; Lopez-Lacomba, J. L.; Ferrer, M. L.; del Monte, F. *J. Mater. Chem.* **2008**, *18* (48), 5933–5940.
(39) Brinker, C. J.; Scherrer, G. W. *Sol−Gel Science*; Gulf Professional Publishing: Houston, TX, 1990.
(40) Pereira, M. M.; Clark, A. E.; Hench, L. L. *J. Biomed. Mater. Res.* **1994**, *28* (6), 693–698.
(41) Fowler, B. O. *Inorg. Chem.* **1974**, *13* (1), 207–214.
(42) Fowler, B. O. *Inorg. Chem.* **1974**, *13* (1), 194–207.
(43) Ohtsuki, C.; Kokubo, T.; Yamamuro, T. *J. Non-Cryst. Solids* **1992**, *143* (C), 84–92.
(44) Andersson, J.; Johannessen, E.; Areva, S.; Baccile, N.; Azãs, T.; Lindãn, M. *J. Mater. Chem.* **2007**, *17* (5), 463–468.
(45) Lao, J.; Nedelec, J. M.; Jallot, E. *J. Phys. Chem. C* **2008**, *112* (25), 9418–9427.
(46) López-Noriega, A.; Arcos, D.; Izquierdo-Barba, I.; Sakamoto, Y.; Terasaki, O.; Vallet-Regí, M. *Chem. Mater.* **2006**, *18* (13), 3137–3144.
(47) Yan, X.; Huang, X.; Yu, C.; Deng, H.; Wang, Y.; Zhang, Z.; Qiao, S.; Lu, G.; Zhao, D. *Biomaterials* **2006**, *27* (18), 3396–3403.
(48) Bretcanu, O.; Samaille, C.; Boccaccini, A. R. *J. Mater. Sci.* **2008**, *43* (12), 4127–4134.
(49) von Doernberg, M. C.; von Rechenberg, B.; Bohner, M.; Grunenfelder, S.; van Lenthe, G. H.; Muller, R.; Gasser, B.; Mathys, R.; Baroud, G.; Auer, J. *Biomaterials* **2006**, *27* (30), 5186–5198.
(50) Hollister, S. J. *Nat. Mater.* **2005**, *4* (7), 518–524.